

HALO STRUCTURES OF GRAVITATIONAL LENS GALAXIES *

JAIYUL YOO¹, CHRISTOPHER S. KOCHANÉK¹, EMILIO E. FALCO², AND BRIAN A. MCLEOD²

accepted for publication in The Astrophysical Journal

ABSTRACT

We explore the halo structure of four gravitational lenses with well-observed, thin Einstein rings. We find that the gravitational potentials are well described by ellipsoidal density distributions in the sense that the best-fit nonellipsoidal models have parameters consistent with their ellipsoidal counterparts. We find upper limits on the standard parameters for the deviation from an ellipse of $|a_3^B/a_0| < 0.023, 0.019, 0.037$, and 0.035 , and $|a_4^B/a_0| < 0.034, 0.041, 0.051$, and 0.064 for SDSS J0924+0219, HE 0435–1223, B 1938+666, and PG 1115+080, respectively. We find that the lens galaxies are at the centers of their dark matter halos, and obtain upper limits for the offset of each center of mass from the center of light of $|\Delta\mathbf{x}| < 0''.004, 0''.005, 0''.009$, and $0''.005$, corresponding to 22, 29, 70, and 23 pc. These limits also exclude the possibility of any significant lopsidedness of the dark matter halos and set an upper limit of $f_{\text{sat}} \lesssim \sqrt{N}\%$ on the mass fraction of massive substructures inside the Einstein ring if they are divided over N satellites. We also explore the properties of galaxies as substructures in groups for the lens PG 1115+080, finding evidence for dark matter halos associated with the galaxies but no evidence for a clear distinction between satellite and central galaxies.

Subject headings: cosmology: observations — dark matter — gravitational lensing — quasars: individual (B 1938+666, HE 0435–1223, PG 1115+080, SDSS J0924+0219)

1. INTRODUCTION

In cold dark matter (CDM) models, a typical virialized object consists of a luminous galaxy centered in a dark matter halo and surrounded by satellites, some of which may contain no stars (e.g., Bullock et al. 2000; Kravtsov et al. 2004). In this paper, we explore three questions about the structure of such halos using four gravitational lenses in which we can accurately measure the structure of the Einstein ring image of the quasar host galaxy.

First, we explore the angular structure of the dark matter halos. The angular structure of luminous early-type galaxies is well-approximated by projected ellipsoidal distributions, or ellipses, albeit with small systematic deviations (Bender et al. 1989; Rest et al. 2001). Considerably less is known about the angular structure of dark matter halos (e.g., Katz 1991; Allgood et al. 2005), particularly after their structure is modified by the dissipative cooling and reheating of the baryons by star formation as the galaxy evolves. This issue is relevant to the halo structures less from an interest in the ellipticity of the halos than from the possibility that strong deviations from an ellipsoidal density distribution may be responsible for the flux ratio anomalies in gravitational lenses (e.g., Mao & Schneider 1998; Zhao & Pronk 2001; Chiba 2002; Metcalf & Zhao 2002) that otherwise provide the strongest evidence for the existence of dark matter substructures in the halos of galaxies (Dalal & Kochanek 2002). Evans & Witt (2003) demonstrated that lens potentials with arbitrary angular structure could reproduce the flux anomalies without the substructures, but Kochanek & Dalal (2004), Yoo et al. (2005), and Congdon & Keeton (2005) demonstrated for several lenses that the deviations in the lens potentials from an el-

lipsoidal distribution are too small to remove the flux anomalies. Here we extend our study of the shape of the gravitational fields in galaxy halos to three more gravitational lens systems.

Second, we explore whether the center of mass of the luminous galaxy is identical to the center of mass of the halo, since most popular halo models assume that luminous galaxies are centered on their dark matter halos (e.g., Seljak 2000; Berlind & Weinberg 2002; Cooray & Sheth 2002). Although it is unlikely that the core of the stellar and dark matter distributions can be offset in a galaxy, potentially there could be some lopsidedness or other effects that would make it invalid to assume that the center of light is the center of mass. Weakening the centering of the halo on the lens galaxy was also one of the factors permitting Evans & Witt (2003) to explain flux ratio anomalies with changes in the lens potential. Small numbers of massive, but dark substructures would also create an offset between the centers of mass and light.

Finally, we explore the halo structure of a galaxy group. It is likely that central and satellite galaxies in a group show significantly different mass-to-light ratios on large scales due to the mass differences between halos associated with each galaxy (e.g., Zheng et al. 2005). This could explain, for example, the increasing evidence that early-type galaxies are heterogeneous in their structure (e.g., Kochanek et al. 2005). Most lens galaxies are members of small galaxy groups, where the other galaxies in the group can perturb the lens through their tidal gravities. If we consider a lens centered on one of the satellite galaxies, then we might plausibly identify the central galaxy if one of the other galaxies in the group has a significantly higher mass-to-light ratio on large scales than the others. If, on the other hand, the structural differences between central and satellite galaxies are small compared to the intrinsic scatter, then no such identification can be made. We can explore these possibilities using lens galaxies in small groups.

We examine these three issues using four gravitational lenses with well-defined Einstein ring images of the quasar host galaxy: SDSS J0924+0219 (Inada et al. 2003; Keeton et al. 2005), HE 0435–1223 (Wisotzki et al. 2000;

* Based on Observations made with the NASA/ESA *Hubble Space Telescope*, obtained at the Space Telescope Science Institute, which is operated by AURA, Inc., under NASA contract NAS5-26555.

¹ Department of Astronomy, The Ohio State University, 140 West 18th Avenue, Columbus, OH 43210; jaiyul@astronomy.ohio-state.edu, ckochanek@astronomy.ohio-state.edu

² Harvard-Smithsonian Center for Astrophysics, 60 Garden Street, Cambridge, MA 02138; efalco@cfa.harvard.edu, bmcleod@cfa.harvard.edu

Morgan et al. 2005; Kochanek et al. 2005), B 1938+666 (King et al. 1997, 1998; Tonry & Kochanek 2000) and PG 1115+080 (Weymann et al. 1980; Courbin et al. 1997; Keeton & Kochanek 1997; Impey et al. 1998; Treu & Koopmans 2002). We use the shape of the Einstein ring formed by quasar host galaxies to accurately constrain the angular structure of the underlying potential (Kochanek et al. 2001; Yoo et al. 2005). In §2 we briefly present the *Hubble Space Telescope* (*HST*) observations of the four lenses followed by a short summary of the lens models in §3. Our main results on the first two questions are presented in §4. We discuss the third question for the galaxy group surrounding PG 1115+080 in §5. We summarize our results in §6.

2. OBSERVATIONS

We analyzed four gravitational lenses (SDSS J0924+0219, HE 0435–1223, B 1938+666, and PG 1115+080) with well-defined, thin Einstein ring images of the quasar host observed at *H*-band (NIC2/F160W) with the Near-Infrared Camera and Multi-Object Spectrograph on the *HST*. The data were reduced and modeled using our standard procedures (McLeod 1997; Lehár et al. 2000), and we extracted the Einstein ring curve as described in Kochanek et al. (2001). The image is fitted by a model consisting of the lens galaxy, the quasar images, and a lensed host galaxy. The lens galaxy and quasar images are then subtracted, and we measure the radius $r(\theta)$ of the Einstein ring as a function of position angle around the lens galaxy. The radius $r(\theta)$ of the ring curve can then be used as a constraint on lens models under the assumption that the isophotes of the host galaxy are close to ellipsoidal.

SDSS J0924+0219 consists of four lensed quasar images of a source at $z_s = 1.524$ produced by an elliptical galaxy at $z_l = 0.393$ (Ofek et al. 2005; Eigenbrod et al. 2005) and the lens is well-separated from nearby galaxies (Inada et al. 2003; Keeton et al. 2005). Eight dithered images of the Einstein ring were obtained on 2004 June 1 for a total integration time of 4640 seconds (Morgan et al. in preparation). We use the image positions from Keeton et al. (2005). The lens is quite isolated and we use only an external shear to model its environment. By isolated, we mean that no nearby object provides higher-order perturbations than an external shear.

The lens system HE 0435–1223 is composed of a four-image lensed quasar at $z_s = 1.689$ (Wisotzki et al. 2000) and an elliptical lens galaxy at $z_l = 0.4546$ (Morgan et al. 2005; Ofek et al. 2005). A spiral-rich group of about 10 galaxies was found within $40''$ and the closest spiral galaxy G22 (SBb) is separated from the lens galaxy by $4.''46$. We use the positions of the lensed images and field galaxies around the lens from the *HST*/ACS images described in Morgan et al. (2005), and the 2560s *HST*/NICMOS image described in Kochanek et al. (2005). As in Kochanek et al. (2005), we model the environment with an external shear and the nearby galaxy G22.

B 1938+666 consists of a normal early-type lens galaxy of redshift $z_l = 0.88$ (Tonry & Kochanek 2000) that produces a two-image system and a four-image system of a radio source of unknown redshift (King et al. 1997). The host galaxy is seen as an almost perfectly circular ring around the lens (King et al. 1998). We analyze the 2816s NIC2 image taken on 1997 October 7. For the radio image positions, we use the 5 GHz observations of King et al. (1997). We allow the registration of radio and optical coordinates to be optimized as part of the fit. The lens is fairly isolated and we model the

environment using only an external shear.

PG 1115+080 consists of four images of a $z_s = 1.72$ quasar lensed by a $z_l = 0.31$ elliptical galaxy (Weymann et al. 1980; Impey et al. 1998). This system belongs to a small group of galaxies producing non-negligible higher-order perturbations. In Yoo et al. (2005), like most previous studies, we modeled the environment as a separate group halo. Here we explore models with halos centered on the galaxy positions provided by Impey et al. (1998). We use the image positions from Impey et al. (1998).

We use a concordance cosmological model with density parameters $\Omega_m = 0.3$, $\Omega_\Lambda = 0.7$ and the Hubble constant $h \equiv H_0/100 \text{ kms}^{-1}\text{Mpc}^{-1} = 0.7$ to calculate angular diameter distances in a Λ CDM universe.

3. LENS MODEL

We use the scale-free potential with arbitrary angular structure

$$\frac{1}{r}\phi(r, \theta) \equiv F(\theta) = a_0 + a_2 \cos 2\theta + b_2 \sin 2\theta + \sum_{m=2}^{\infty} \frac{a_0}{1-4m^2} a_{2m}^q \cos 2m(\theta - \theta_L) + \sum_{m=3}^{\infty} [\Delta a_m \cos m\theta + \Delta b_m \sin m\theta], \quad (1)$$

as our lens model. The model has a flat rotation curve, which also seems to be true of the typical lens galaxy (e.g., Treu & Koopmans 2002; Rusin & Kochanek 2005). This lens model has been used extensively in other studies (Zhao & Pronk 2001; Evans & Witt 2001, 2003; Kochanek et al. 2001; Wucknitz 2002; Yoo et al. 2005; Congdon & Keeton 2005). The model parameters are a_0 , a_2 , b_2 , Δa_m and Δb_m with $m \geq 3$. The coefficients a_{2m}^q for the ellipsoidal part of the surface density of the lens galaxy are determined from the quadrupole moment of the galaxy defined by the model parameters as

$$a_2^q = -\frac{3}{a_0} (a_2 \cos 2\theta_L + b_2 \sin 2\theta_L), \quad (2)$$

and the major axis orientation, $\theta_L = 0.5 \tan^{-1}(b_2/a_2)$. Note that the $m = 1$ terms in this potential are degenerate with a shift in the source position and can be neglected. The standard parameters for the deviation of the mass density of the lens galaxy from an ellipsoid are $a_m^B/a_0 \equiv (1-m^2)\Delta a_m/a_0$ and $b_m^B/a_0 \equiv (1-m^2)\Delta b_m/a_0$ for $m \geq 3$ (e.g., Bender & Möllenhoff 1987; Bender et al. 1989). We consider either ellipsoidal models ($\Delta a_m \equiv \Delta b_m \equiv 0$) or nonellipsoidal models where $\Delta a_m \neq 0$ and $\Delta b_m \neq 0$ for $m \leq 5$. In either type of model, we expand the ellipsoid to order $m = 5$, beyond which higher-order coefficients and deviations are negligible for the relatively round lens galaxies (of axis ratio $q_L \simeq 1$) we consider here.

We also include two sources of external perturbations. The first is an independent external shear due to objects distant from the lens or along the line-of-sight (Keeton et al. 1997). Thus, we add a term to the potential

$$\phi_\gamma(r, \theta) = \frac{1}{2} \gamma r^2 \cos 2(\theta - \theta_\gamma) \equiv r^2 G_\gamma(\theta), \quad (3)$$

with two free parameters for the shear amplitude γ and orientation θ_γ . The second source of perturbations are galaxies near the main lens that can produce higher-order perturbations beyond an external shear (e.g., Keeton & Zabludoff

TABLE 1
BEST-FIT MODELS

	SDSS J0924+0219		HE 0435-1223		B 1938+666	
Parameter	Ellipsoidal	Nonellipsoidal	Ellipsoidal	Nonellipsoidal	Ellipsoidal	Nonellipsoidal
q_s	0.86 ± 0.06	0.84 ± 0.16	0.47 ± 0.02	0.51 ± 0.06	0.56 ± 0.10	0.56 ± 0.18
$\theta_s(\text{deg})$...	-24.4 ± 14.3	-28.0 ± 22.7	-3.9 ± 2.0	-6.1 ± 3.2	-71.2 ± 9.3	-71.2 ± 23.3
γ	0.058 ± 0.013	0.058 ± 0.023	0.035 ± 0.003	0.065 ± 0.003	0.026 ± 0.004	0.026 ± 0.007
$\theta_\gamma(\text{deg})$..	65.6 ± 0.9	62.0 ± 3.5	-60.2 ± 5.1	-68.3 ± 4.1	33.1 ± 14.0	33.3 ± 15.6
γ_g	—	—	0.040 ± 0.001	0.042 ± 0.003	—	—
$r_g(\text{arcsec})$	—	—	$\equiv 4.46$	$\equiv 4.46$	—	—
$\theta_g(\text{deg})$..	—	—	$\equiv -144.7$	$\equiv -144.7$	—	—
$x_L(\text{arcsec})$	-0.001 ± 0.001	-0.001 ± 0.003	-0.003 ± 0.002	-0.001 ± 0.003	-0.007 ± 0.007	-0.007 ± 0.007
$y_L(\text{arcsec})$	0.001 ± 0.001	-0.004 ± 0.003	0.000 ± 0.001	0.001 ± 0.003	0.004 ± 0.007	0.004 ± 0.009
q_L	0.87 ± 0.01	0.85 ± 0.02	0.62 ± 0.01	0.55 ± 0.01	0.89 ± 0.02	0.89 ± 0.01
$\theta_L(\text{deg})$..	-68.1 ± 7.3	-67.2 ± 9.8	-14.3 ± 9.1	-10.5 ± 9.4	-54.9 ± 8.5	-54.5 ± 10.2
a_0	0.88 ± 0.01	0.88 ± 0.02	1.21 ± 0.01	1.21 ± 0.01	0.46 ± 0.01	0.46 ± 0.01
$10^2 a_2$	-1.4 ± 0.2	-1.6 ± 0.4	8.3 ± 0.4	11.1 ± 0.5	-0.3 ± 0.3	-0.3 ± 0.4
$10^2 b_2$	-1.4 ± 0.4	-1.7 ± 1.1	-4.5 ± 0.4	-4.2 ± 0.7	-0.8 ± 0.1	-0.8 ± 0.3
$10^3 \Delta a_3$	$\equiv 0$	-0.9 ± 2.5	$\equiv 0$	2.1 ± 3.3	$\equiv 0$	0.0 ± 4.8
$10^3 \Delta b_3$	$\equiv 0$	-2.2 ± 3.8	$\equiv 0$	1.4 ± 4.7	$\equiv 0$	0.1 ± 4.3
$10^3 \Delta a_4$	$\equiv 0$	0.8 ± 3.0	$\equiv 0$	2.9 ± 3.3	$\equiv 0$	0.0 ± 2.1
$10^3 \Delta b_4$	$\equiv 0$	1.2 ± 3.3	$\equiv 0$	0.1 ± 6.6	$\equiv 0$	0.0 ± 1.7
$10^4 \Delta a_5$	$\equiv 0$	-1.7 ± 11.9	$\equiv 0$	0.1 ± 8.4	$\equiv 0$	0.1 ± 1.2
$10^4 \Delta b_5$	$\equiv 0$	-1.1 ± 15.6	$\equiv 0$	0.1 ± 5.3	$\equiv 0$	0.0 ± 1.3
χ^2_{ring}	54.9	47.8	20.9	15.9	4.1	4.1
χ^2_{image}	0.3	0.1	0.2	0.2	2.3	2.3
χ^2_{lens}	0.3	1.8	1.3	0.4	0.7	0.7
χ^2_{tot}	55.5	49.6	22.5	16.4	7.1	7.1
N_{dof}	69	63	70	64	66	60
$F\text{-Test}(\%)$	—	93.4	—	35.9	—	70.4

NOTE. — The best-fit ellipsoidal and nonellipsoidal models. Only astrometric constraints are used in the fits. Angles are standard position angles while the lens position and the coefficients of the lens potential are calculated in Cartesian coordinates in which x -direction is toward the West. The model parameters are the axis ratio q_s and major-axis position angle θ_s of the source, the external shear (γ , θ_γ), the shear perturbation γ_g produced by a nearby galaxy at (r_g , θ_g), the position of the lens (x_L , y_L), the axis ratio q_L and major-axis position angle θ_L of the lens, the ellipsoidal lens potential $\{a_0, a_2, b_2\}$, and the higher-order deviations Δa_m and Δb_m for $m = 3, 4, 5$ from an ellipsoid.

2004; Kochanek et al. 2005). We approximate these galaxies by the potential,

$$\phi_{\text{env}}(r, \theta) \simeq r \sum_{m=1}^{\infty} a_m^g \cos m(\theta - \theta_g) + r^2 \sum_{m=1}^{\infty} b_m^g \cos m(\theta - \theta_g) \\ \equiv r F_{\text{env}}(\theta) + r^2 G_{\text{env}}(\theta), \quad (4)$$

where the coefficients a_m^g and b_m^g for $m \leq 3$ are determined by minimizing the difference between this model and the deflection produced by a singular isothermal sphere (SIS), $\phi_{\text{SIS}}(\mathbf{r}) = b_g |\mathbf{r} - \mathbf{r}_g|$, where b_g is the Einstein radius of the nearby galaxy and \mathbf{r}_g is its position vector from the lens center. The approximation is accurate to within $0''.001$ over an annulus of width $1''$ encompassing the Einstein ring for the closest perturbing galaxy in our sample (galaxy G22 in HE 0435-1225, which is $4''.5$ from the lens galaxy).

The total potential is $\phi(r, \theta) = r[F(\theta) + F_{\text{env}}(\theta)] + r^2[G_{\text{env}}(\theta) + G_\gamma(\theta)]$, which may include contributions from several nearby galaxies. For an ellipsoidal host galaxy with a monotonically decreasing surface brightness, the Einstein ring curve defined by the peak surface brightness of the Einstein ring as a function of angle θ going around the lens galaxy is simply

$$r(\theta) = \frac{\mathbf{h} \cdot \mathbf{S} \cdot \mathbf{t} + \mathbf{u}_o \cdot \mathbf{S} \cdot \mathbf{t}}{\mathbf{t} \cdot \mathbf{S} \cdot \mathbf{t}}, \quad (5)$$

where $\mathbf{h} \equiv (F + F_{\text{env}})\hat{\mathbf{e}}_r + (F' + F'_{\text{env}})\hat{\mathbf{e}}_\theta$, the source plane tangent vector is $\mathbf{t} = \mathbf{M}^{-1} \cdot \hat{\mathbf{e}}_r = (1 - 2G_{\text{env}} - 2G_\gamma)\hat{\mathbf{e}}_r - (G'_{\text{env}} + G'_\gamma)\hat{\mathbf{e}}_\theta$,

\mathbf{M}^{-1} is the inverse magnification tensor, the source center is \mathbf{u}_o , and \mathbf{S} is the two-dimensional shape tensor of the source with axis ratio q_s and position angle of its major axis θ_s (see Kochanek et al. 2001; Yoo et al. 2005).

For each lens we fit the image positions, the lens galaxy position, and the Einstein ring curve using a simple χ^2 statistic,

$$\chi^2(\mathbf{p}) = \sum_i^{N_{\text{img}}} \frac{[\mathbf{u}_o - \mathbf{u}_i(\mathbf{p})] M_i|^2}{\sigma_{i,\text{img}}^2} + \sum_i^{N_{\text{ring}}} \frac{|r(\theta_i) - r(\theta_i; \mathbf{p})|^2}{\sigma_{i,\text{ring}}^2}, \quad (6)$$

where $\sigma_{i,\text{img}}$ and $\sigma_{i,\text{ring}}$ are the uncertainties in the i -th image position and the i -th Einstein ring radius, respectively. To allow rapid parameter searches, we use this source plane statistic for the χ^2 weighted by magnification $M = |\mathbf{M}|$ to approximately correct for the difference between deviations on the source and image planes. Our fiducial ellipsoidal model has 11 free parameters, \mathbf{p} ; the source position is $\mathbf{u}_o = (u_x, u_y)$, the axis ratio q_s and major-axis position angle θ_s of the source, the ellipsoidal lens potential $\{a_0, a_2, b_2\}$, the position of the lens (x_L, y_L), and the external shear amplitude and direction (γ, θ_γ). In addition, there is one parameter $\gamma_g \equiv b_g/2r_g$ for each nearby galaxy with observed position $\mathbf{r}_g = (r_g, \theta_g)$ that may be added depending on the environment of the lens galaxy. Although flux ratios can provide additional constraints, they can be changed by dust extinction (e.g., Falco et al. 1999), microlensing (e.g., Chiba et al. 2005), and perturbations by substructure (e.g., Kochanek & Dalal 2004), so we will use only astrometric constraints. We used the

Levenberg-Marquardt method to minimize the χ^2 statistic of a given model and to estimate the parameter uncertainties, and we checked the convergence of our solutions by repeating the minimization with a wide range of initial parameters and whether we have reached a global minimum by using the complementary downhill simplex method (e.g., Press et al. 1992).

4. THE STRUCTURE OF LENS GALAXIES

In this section, we analyze the lens systems to investigate whether the lens galaxies show any evidence for nonellipsoidal structures in their density distribution. As in Yoo et al. (2005), we first fit each lens as an ellipsoid centered on the center of brightness of the lens galaxy and then fit it allowing deviations from ellipsoidal structure or offset positions. The significance of the changes can be evaluated by using the F -test to estimate the significance of the improvements to the fit from adding the additional structural parameters and by considering the scale of the deviations from ellipsoidal structure. The best-fit parameters and the F -test results for each model and each lens galaxy are presented in Table 1. Each lens is modeled with the environmental components (shear, nearby galaxies) described in §2. We focus on higher order ($m \geq 3$) angular structure in §4.1 and on the match between the center of mass and the center of light in §4.2.

4.1. Angular Structure

Our basic result is that SDSS J0924+0219, HE 0435–1223 and B 1938+666 appear to be ellipsoids, as we had previously found for PG 1115+080 (Yoo et al. 2005). In all four cases, the improvement in the goodness of the fit from adding the $m = 3 - 5$ terms to the potential is statistically insignificant. The results of the fits are summarized in Table 1.

Figure 1 illustrates the differences in the critical lines and isodensity contours for the ellipsoidal and nonellipsoidal models of the three lenses. Figure 2 displays the values of the center of mass offsets and the higher order deviations b_m^B/a_0 ($m = 3, 4, 5$) from an ellipsoid. In Table 1, we quantify the difference of the two best-fit ellipsoidal and nonellipsoidal models by providing the F -test probability for the nonellipsoidal model being consistent with the ellipsoidal model. In none of the lenses do the additional structural parameters of the nonellipsoidal model improve the fits.

Although we generally ignore the constraints on the flux ratios in this paper, we note that the best-fit ellipsoidal models reproduce the observed flux ratios except for the images with flux anomalies that are probably due to substructure or stellar microlensing. For example, the flux anomaly A_1/A_2 of PG 1115+080 turns out to be due to the stellar microlensing (Chiba et al. 2005). The image D of SDSS J0924+0219 and the images A and C of HE 0435–1223 also show deviations of predicted compared to observed fluxes while the global lens models in both cases provide a reasonable fit to the image positions and the flux ratios of the rest of the images. Since the magnification is more sensitive to the higher order structure in the potential, the best-fit nonellipsoidal models using only astrometric constraints fit the observed flux ratios of the anomalous images poorly. However, even if we impose the flux ratio constraints including the anomalies, the best-fit parameters change little from those for the ellipsoidal model, and it is simply impossible to fit the flux ratios while simultaneously obtaining a good fit to each Einstein ring. We consider models based only on the astrometric constraints in the rest of this paper.

Ellipsoidal models fit the observed image positions and the Einstein ring of SDSS J0924+0219 well with $\chi_{\text{dof}}^2 = 0.80$. While a slightly better fit with $\chi_{\text{dof}}^2 = 0.79$ is found using the nonellipsoidal model, the F -test probability that the additional variables were unnecessary is 93.4%, so the astrometric constraints from the Einstein ring strongly favor the ellipsoidal model for the lens galaxy of SDSS J0924+0219 over nonellipsoidal models. Contrary to Eigenbrod et al. (2005), we have no difficulty finding a model that simultaneously fits the quasar images and the Einstein ring. The difference probably arises because Eigenbrod et al. (2005) compared model parameters from two separate fits to each constraint rather than fitting both constraints simultaneously.

HE 0435–1223 is also well fitted by the ellipsoidal model with $\chi_{\text{dof}}^2 = 0.32$ (see Fig. 1). In fact, we overfit the data and/or the uncertainties in the Einstein ring curve are overestimated by 76%. The ellipsoidal model with a nearby SIS and an external shear provides a fit consistent with the recent measurements of the image time delays (Kochanek et al. 2005), and the parameters of the best-fit nonellipsoidal model are consistent with those of the ellipsoidal model. In addition to the F -test indicating that the additional variables of this nonellipsoidal model are unnecessary, the best-fit nonellipsoidal model requires a high external shear of $\gamma = 0.065$ compared to 0.035 for the ellipsoidal model. Considering that we have taken out the contribution from the nearby galaxy G22, it is unphysical to have external perturbations of $\sim 7\%$. The high amplitude of the external shear in the nonellipsoidal model compensates for the higher order deviations of the lens potential from an ellipsoid.

The lens system B 1938+666 exhibits doubly lensed (*open squares*) and quadruply (*open triangles*) lensed radio images whose sources are two radio lobes rather than a central core (King et al. 1997). Note that the double radio images are offset from the Einstein ring. For this lens, we therefore include two additional source positions for the radio images offset from the center of the host galaxy producing the Einstein ring. The nearly circular Einstein ring rules out any significant higher order deviations in nonellipsoidal models, and the best-fit nonellipsoidal model is consistent with the ellipsoidal model (see Fig. 2).

4.2. Center of Dark Matter Halos

In the previous subsection we constrained the position of the lens galaxy to agree with the position of the luminous galaxy seen in the *HST* images. This is the standard assumption of almost all lens models. In principle, the center of mass could differ from the center of light if the halo were genuinely offset from the stars, if the halo were significantly lopsided, or if there were any sufficiently massive dark substructures inside the Einstein ring. To test these possibilities, we drop the constraints on the lens position and repeat the optimization of the ellipsoidal models to estimate the offset (x_L, y_L) of the center of mass from the lens galaxy. Physically it seems unlikely that the galaxy light can be significantly offset from the dark matter halo on galaxy scales, and this is borne out by these results. We find that the center of mass can be offset from the center of light by only $\Delta_{\text{cm}} = 0''.001 \pm 0''.003, 0''.003 \pm 0''.004, 0''.008 \pm 0''.009$, and $0''.001 \pm 0''.002$ for SDSS J0924+0219, HE 0435–1223, B 1938+666, and PG 1115+080, respectively. These correspond to physical offsets of $\Delta_{\text{cm}} = 5.4 \pm 16.3, 17.4 \pm 23.1, 61.9 \pm 69.6$, and 4.6 ± 9.1 pc. The nonellipsoidal models only increase the uncertainties in the offsets by roughly a factor

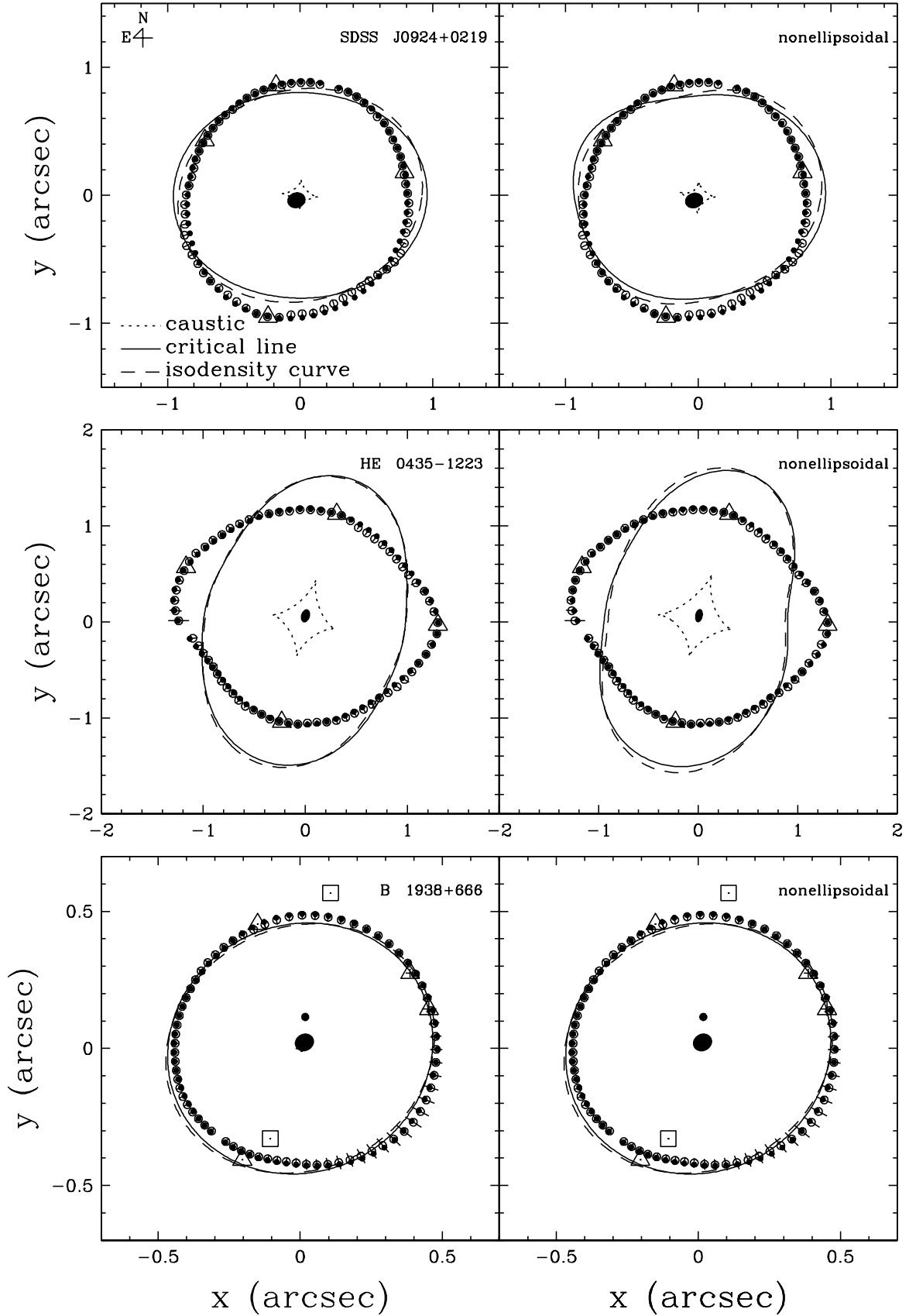


FIG. 1.— Best-fit ellipsoidal (*left panels*) and nonellipsoidal (*right panels*) models. Open circles and triangles represent the observed positions of the Einstein ring and the lensed images. Positional uncertainties in observations are indicated by the lines passing through each symbol. Filled circles show the Einstein ring position predicted by best-fit models, while the filled ellipse at the center shows the predicted position, ellipticity, and position angle of the source. The caustic, the critical line, and the isodensity curve of the ellipsoidal model are shown as dotted, solid, and dashed lines, respectively. Open squares in the bottom panels represent the observed positions of the two additional lensed images, and the small filled circle just above the center shows the predicted position of the additional source for these images. Note that the other source position is nearly identical to the center of the host galaxy ($|\Delta u| \simeq 0''.023$).

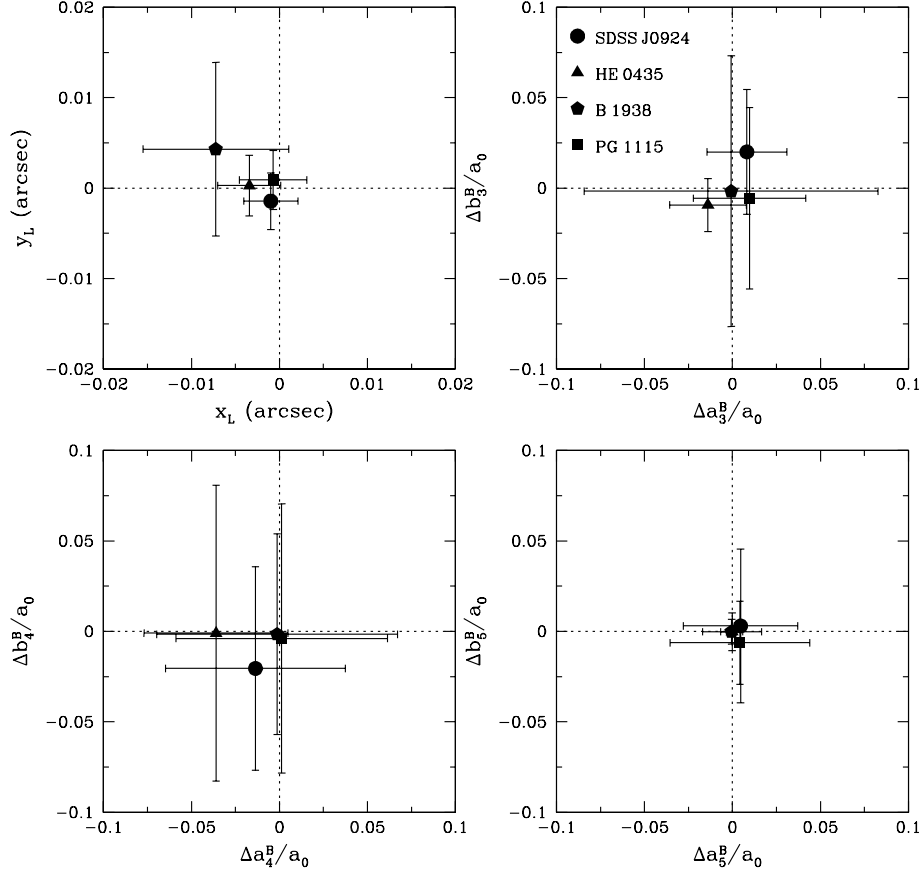


FIG. 2.— Center of mass offsets (*top left*) and the higher-order deviation coefficients of the best-fit nonellipsoidal models.

of 1.5 and provide upper limits consistent with the values of the offsets. For a typical dark matter fraction inside the Einstein ring of $\epsilon \simeq 30\%$ (Koopmans & Treu 2003; Rusin et al. 2003b), the offset in the center of mass of the dark matter halo is related to the offset in the center of mass by $\Delta_{\text{dm}} \simeq \Delta_{\text{cm}}/\epsilon$, so the limits on the offset of the dark matter halo are somewhat weaker. Note that this co-location of the stars and the halo may not hold in clusters. For example, models of the cluster lens SDSS J1004+4112 require an offset of $\gtrsim 5.7$ kpc between the cD galaxy and the center of the cluster potential (Oguri et al. 2004), and there is some evidence that cD galaxies are not at rest with respect to the rest frame defined by the other cluster galaxies (e.g., van den Bosch et al. 2005).

The offsets also test the lopsidedness of dark matter halos and the existence of massive dark substructures. The luminous galaxies show no evidence for lopsidedness, because they are well modeled by ellipsoidal de Vaucouleur profiles. Since dark matter halos are also supported by random particle motions, they should also have difficulty supporting a lopsided density structure, and this is borne out by the tight limits on Δ_{dm} . Finally, the lack of an offset also sets a limit on the existence of massive dark substructures. Given a typical subhalo mass function, most massive substructures dominate the total mass contained in substructure (Klypin et al. 1999; Moore et al. 1999; Taylor & Babul 2004; Gao et al. 2004; Zentner et al. 2005). If we add a single ob-

ject whose mass is fraction f_{sat} of the mass inside the Einstein ring at radius r_{sat} for the lens galaxy, it would shift the center of mass by $\Delta_{\text{cm}} = f_{\text{sat}} r_{\text{sat}}$. Thus, we have a limit that $f_{\text{sat}} \lesssim \Delta_{\text{cm}}/\langle r_{\text{sat}}^2 \rangle^{1/2}$ where $\langle r_{\text{sat}}^2 \rangle^{1/2}$ is the rms distance of the satellites inside the Einstein ring from the lens center. Crudely, $\langle r_{\text{sat}}^2 \rangle^{1/2} \simeq b$, the Einstein radius, so $f_{\text{sat}} \lesssim 1\%$. Adding additional satellites only weakly affects the limits, increasing the limit on f_{sat} by \sqrt{N} for N equal mass satellites. This strong sensitivity to massive substructures is presumably one of the reasons that it is almost impossible to model lenses like MG J0414+0534 with visible satellites using only a central potential (e.g., Ros et al. 2000; Trotter et al. 2000).

5. GROUP VS. GALAXY HALOS IN PG 1115+080

In the halo model that describes the relation of galaxies and dark matter, a luminous central galaxy is located at the center of dark matter halo and the satellite galaxies are distributed around the central galaxy (e.g., Berlind & Weinberg 2002; Kravtsov et al. 2004). In §4.2, we found that visible lens galaxies must be centered on their halos, and that they generally lack massive substructures. If, however, we consider a lens consisting of a galaxy in a group, like PG 1115+080, then we can explore the relationship between central and satellite galaxies. This is potentially important because the time delay measurements for PG 1115+080 (Schechter et al. 1997) require a main lens galaxy with almost no dark mat-

ter at the concordance value of the Hubble constant $H_0 = 72 \text{ km s}^{-1} \text{ Mpc}^{-1}$ (Kochanek 2003), in marked contrast to the typical lens galaxies, which seem to have a significant dark halo (e.g., Treu & Koopmans 2002; Rusin & Kochanek 2005). This case suggests that the structures of early-type galaxies are heterogeneous. One possible interpretation of this heterogeneity is that the primary lens of PG 1115+080 is a satellite lens galaxy of the group that has been stripped of most of its dark matter. In the context of the halo model, this implies that one of the other visible galaxies around PG 1115+080 must be the central galaxy of the group, and it should show a significantly higher mass-to-light ratio than the other galaxies, all of which are satellites. In this section, we attempt to interpret PG 1115+080 within this theoretical picture.

5.1. The Environment of PG 1115+080

Figure 3 shows the environment of PG 1115+080. Earlier models with an independent external shear or an SIS external perturber consistently indicate that the lens has a $\sim 10\%$ shear perturbation associated with its parent group, with weak evidence that the group halo should be located near the luminosity weighted position of the nearby galaxies (Schechter et al. 1997; Keeton & Kochanek 1997; Courbin et al. 1997; Impey et al. 1998; Zhao & Pronk 2001; Kochanek & Dalal 2004; Yoo et al. 2005). The galaxies G1, G2 and G3 are comparable in luminosity to the main lens galaxy, and the less luminous galaxy G14 is the closest. To estimate the perturbations produced by each galaxy, we use the I -band luminosities L of the nearby galaxies in Table 2 (Impey et al. 1998) and the Faber-Jackson relation to estimate their stellar velocity dispersions $\sigma_* \propto L^{1/4}$ and the Einstein radii $b \propto \sigma_*^2$ ($L \propto \sigma_*^4 \propto b^2$). Scaling all the galaxies based on

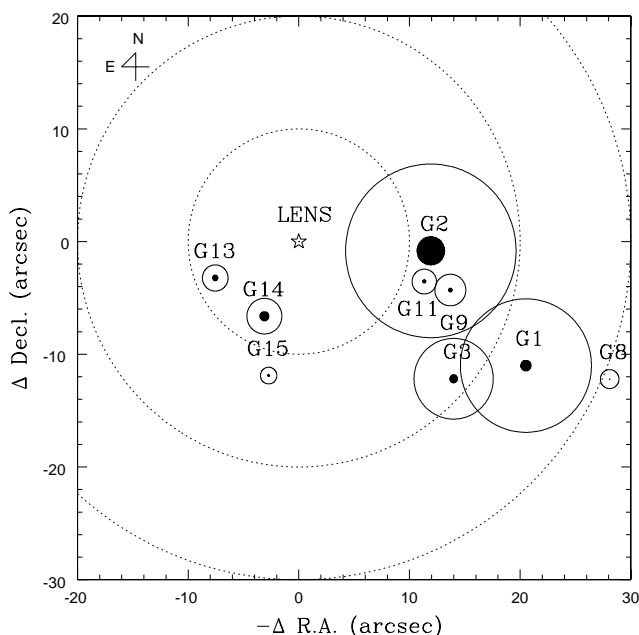


FIG. 3.— The environment of PG 1115+080. The nearby galaxies are represented by the labeled circles, where the sizes of the circles are proportional to the perturbation produced by each galaxy. Solid circles are for the external shear, and filled circles are for the higher-order perturbations. The dotted concentric circles centered on the main lens galaxy are reference circles with radii of $10''$, $20''$, and $30''$.

TABLE 2
GALAXY ENVIRONMENT OF PG 1115+080

Object	$I(\text{mag})$	$r_g(\text{arcsec})$	$\theta_g(\text{degrees})$	γ_g
Lens.....	18.55 ± 0.50	$\equiv 0$	—	—
G1.....	17.85 ± 0.01	23.285	241.80	0.030
G2.....	18.73 ± 0.04	11.957	266.05	0.039
G3.....	19.44 ± 0.02	18.543	228.97	0.018
G8.....	21.52 ± 0.08	30.624	246.52	0.004
G9.....	19.44 ± 0.02	14.352	252.57	0.007
G11.....	22.98 ± 0.34	11.881	252.62	0.006
G13.....	23.70 ± 0.10	8.214	113.16	0.006
G14.....	23.30 ± 0.10	7.313	154.82	0.008
G15.....	23.80 ± 0.10	12.198	167.09	0.004

NOTE. — Galaxy positions are relative to the lens. We use the I -band luminosities and the Faber-Jackson relation to estimate the relative amplitudes of the external shear γ_g produced by each galaxy. The nonlinear perturbations are smaller than γ_g by r_g . The positions and luminosities are from Impey et al. (1998).

the luminosity and Einstein radius of the main lens galaxy, we then compute the relative amplitudes of the external shear $\propto b/r_g$ and the nonlinear perturbation $\propto b/r_g^2$ produced by each galaxy given its distance r_g from the lens (see Table 2). As illustrated in Figure 3, the luminous galaxies G1, G2, and G3 dominate the perturbations while the nearby, less luminous galaxies G13 and G14 make a non-negligible contribution.

We first test whether putting mass only at the positions of the visible galaxies can adequately fit the data, initially with no extra external shear. The galaxy positions are measured to such high accuracy that we fix the observed position $\mathbf{r}_g = (r_g, \theta_g)$ for each galaxy, while we vary their Einstein radii b_i through the free parameter $\gamma_{g,i}$. We started with a model using just the three bright galaxies G1, G2, and G3. Figure 4 shows the best-fit models. The three-galaxy environment fits the data quite poorly compared to standard models with a group halo centered near the center of light of the galaxies ($\Delta\chi^2 \simeq 28$). Only if we allow a large, independent external shear ($\gamma \gtrsim 0.07$) can we obtain a good fit. However, when we include the next leading perturber, G14, the goodness of fit is somewhat better ($\Delta\chi^2 \simeq -5$) than for the fit with a halo unassociated with the visible galaxies. Note however that this new model has one more degree of freedom compared to the standard model, so the improvement in the fit is physically interesting but not statistically significant. Including the fifth most important galaxy, G13, hardly changes the goodness-of-fit, and the Einstein radii of the galaxies change little (although there are mass degeneracies between G1 and G2/G3). If we add an independent external shear to the four or five galaxy models, the estimated shear amplitude is small ($\gamma \simeq 0.01$), and the goodness-of-fit and the Einstein radii of the galaxies remain unchanged. The addition of any more nearby galaxies simply contributes to the external shear γ because they produce negligible higher-order perturbations. Therefore, we adopt the four-galaxy model of G1, G2, G3, and G14 with an external shear of amplitude $\gamma < 0.01$ as our fiducial model for the environment in PG 1115+080. Next we address whether the masses of these galaxies show any correlations that test the structures of their halos.

5.2. Halo Structure of the Galaxy Group of PG 1115+080

Our parameter for each galaxy, $\gamma_g \propto M(< r_g)/r_g^2$, is proportional to the projected mass $M(< r_g)$ of each galaxy out to the

distance of the galaxies r_g from the lens. Based on the halo model, our working hypothesis is that one of these four galaxies is the central galaxy of the halo and should have different halo properties than the other satellite galaxies.

For any fixed assumption about the halo structure and assuming the galaxies have similar mass-to-light ratios, we would expect to see a correlation between these mass estimates b_i and the galaxy luminosities L_i . If there is a central galaxy with a very different halo mass than the satellite galaxies, then it should be identifiable as the galaxy least in agreement with the correlation of the other galaxies. We first consider two limiting cases in which the halos are either all truncated on a scale less than the distance to the lens or where all halos conspire to have flat rotation curves out to the distance to the lens. The Einstein radius is $b_i^{\text{est}} \propto L_i^{1/2}$ in both cases while the shear amplitude produced by each galaxy is $\gamma_i = b_i^2/r_{g,i}^2$ in the former case and $\gamma_i = b_i/2r_{g,i}$ in the latter case. We include the correlation by adding a term to the fit statistic of the form

$$\Delta\chi_{M-L}^2 = 2(N_{\text{gal}} - 1) \ln \sigma + \sum_{i=1}^{N_{\text{gal}}} \frac{[\ln b_i - \ln b_i^{\text{est}}(L_i)]^2}{\sigma^2}, \quad (7)$$

where σ is the logarithmic scatter in the correlation and $N_{\text{gal}} = 4$.

Figure 5 compares the two mass models with and without an external shear γ . When we include the shear, we use a prior constraint of $\gamma = 0.00 \pm 0.01$ (based on the previous four galaxy model). The model assuming extended halos fits the data slightly better ($\Delta\chi^2 \simeq 2$) than the point-mass model regardless of the assumed scatter or the addition of the external shear. The logarithmic scatter of the correlation is $\sigma \simeq 0.5$ for the best-fit model, and will give $\sim 65\%$ fractional dif-

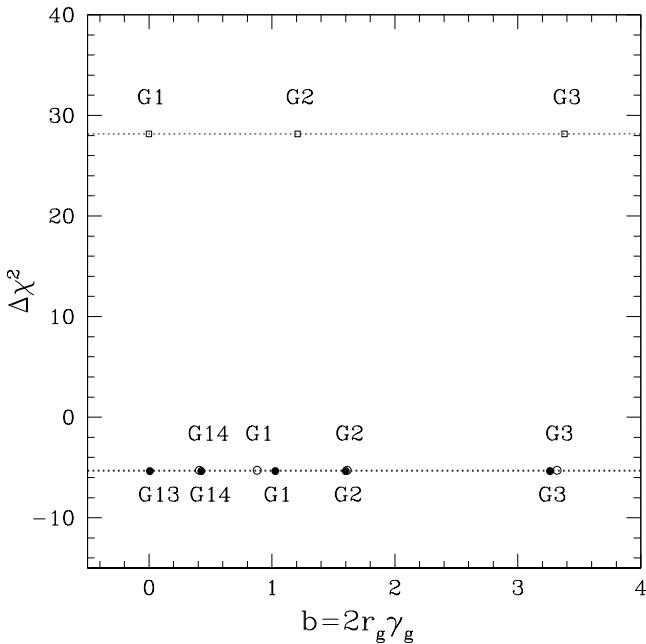


FIG. 4.— Best-fit models for the environment in PG 1115+080. The goodness-of-fit relative to the best-fit model with a group halo unassociated with the visible galaxies is shown with the Einstein ring radii of galaxies in each model. The environment is approximated as three (*open squares*), four (*open circles*), and five nearby galaxies (*filled circles*) from top to bottom. Note that the models with four and five nearby galaxies are degenerate.

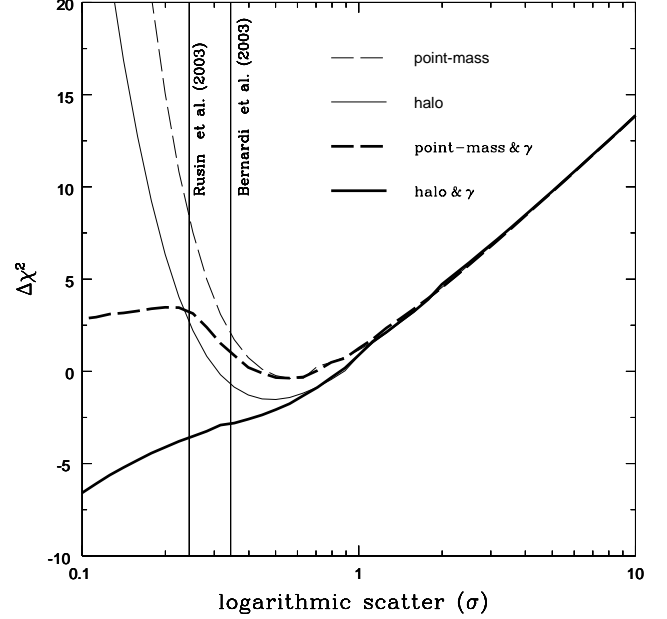


FIG. 5.— Mass models for the galaxy environment. We assume a Faber-Jackson relation $L \propto b^2$ with a natural logarithmic scatter σ . We show the goodness-of-fit as a function of the scatter for each mass model relative to the best-fit model of the four nearby galaxies with arbitrary mass. Solid lines show the results for galaxies with extended halos, and dashed lines show the results for point-mass halos. The light curves allow no additional external shear while the thick lines allow a small external shear. Since the mass scales of the galaxies are not in perfect agreement with the correlation in the mass models without an external shear, the difference in χ^2 becomes substantial as a tight correlation is imposed ($\sigma \ll 1$). The mass models with an external shear can perfectly agree with the correlation, and the $\Delta\chi^2$ is controlled by the assumed prior on the scatter. Two vertical lines show the logarithmic scatters found in the SDSS for nearby elliptical galaxies (Bernardi et al. 2003) and for ensembles of lens galaxies (Rusin et al. 2003a).

ferences. Note that there is little evidence of a useful correlation, but the scatter is not significantly different from the Faber-Jackson relation between the luminosity L and the central velocity dispersion σ_* observed for early-type galaxies in the SDSS ($\sigma \simeq 0.34$ in our units, Bernardi et al. 2003) or that measured from ensembles of lens galaxies ($\sigma \simeq 0.24$, Rusin et al. 2003a). When an external shear is allowed, it turns out that there is degeneracy between the external shear and the mass models for the four galaxies such that all the galaxies can perfectly agree with the assumed correlation, and the results are controlled by our prior on the scatter. The extended halo model requires $\gamma \simeq 2\%$ to fit the data with all galaxies on the correlation, while the point-mass model needs $\gamma \simeq 4\%$.

As our next experiment, we allow one of the four galaxies to have an arbitrary mass while imposing the correlation on the rest of the three galaxies ($N_{\text{gal}} = 3$). Unfortunately, no single galaxy stands out, and the best-fit models without an external shear again require large intrinsic scatters $\sigma \simeq 0.5$. When an external shear is allowed in the model, the external shear can always compensate for the shear produced by the galaxies due to the degeneracy between the external shear and the mass models, and no models are significantly better than the models with the four galaxies in the correlation.

6. SUMMARY

In this paper we explored the structure of halos using four gravitational lenses with well-defined Einstein ring images of the quasar host galaxies. Adopting a scale-free potential with arbitrary angular structure, we considered both ellipsoidal and nonellipsoidal gravitational potentials, searching for any deviation from an ellipsoidal potential. Based on the astrometric constraints, none of the additional free parameters represents an improvement over the best-fit ellipsoidal models, and the best-fit nonellipsoidal models are consistent with their ellipsoidal counterparts. Furthermore, imposing the observed flux ratios as constraints does not alter the results. Anomalous flux ratios can not be eliminated by changing the central potential. The angular structures of all four lens systems are consistent with ellipsoidal models.

We also investigated the offset of the center of mass of the lenses from the measured center of light by dropping the constraints that the lens is centered on the visible galaxy. We find that the offsets are required to be $\Delta_{\text{cm}} \lesssim 10$ pc. This roughly implies that the dark matter halos can be offset by at most $\Delta_{\text{dm}} \simeq \Delta_{\text{cm}}/\epsilon \lesssim 30$ pc, where $\epsilon \simeq 30\%$ is a typical fraction of dark matter inside the Einstein ring. This may be markedly different from clusters in which the cD galaxy can be significantly offset from the center of the cluster potential. Dark substructures of mass fraction f_{sat} could also shift the center of mass if there are few of them, and this allows us to set a limit of $f_{\text{sat}} \lesssim \sqrt{N}\%$ for N equal mass substructures inside the Einstein ring. This limit is not tight enough to represent a conflict with either theoretical (Taylor & Babul 2004; Gao et al. 2004; Zentner et al. 2005) or observational (Dalal & Kochanek 2002) estimates of the substructure fraction.

Finally, we explored the environment of PG 1115+080 to study the halo structure of its parent group under the assumption that the individual dark matter halos are centered on the nearby luminous galaxies. We focused on the four galaxies G1, G2, G3, and G14 producing the largest perturbations, since the other nearby galaxies produce negligible higher-order perturbations and have effects degenerate with an independent external shear. Placing the mass solely on these galaxies can fit the data, but we find only weak evidence for any systematic correlation between the mass and the luminosity. Models assuming the galaxies have extended halos on the scale of their separations are slightly better than those where they do not, but the scatter in the correlation between the Einstein radius and I -band luminosity must be $\sim 65\%$. This is comparable to that implied by Faber-Jackson relation observed for nearby galaxies or for lens galaxies. We also found no evidence for a marked difference between one of the galaxies (the “group halo central galaxy”) and the others (satellite galaxies). The rapid convergence of the perturbations from nearby galaxies to a single external shear probably means that lenses like PG 1115+080 provide an insufficient number of constraints to test the hypothesis of the halo model in detail.

This research has been supported by grants HST-GO-7495, 9375, and 9744 from the Space Telescope Science Institute, which is operated by the Association of Universities for Research in Astronomy, Inc., under NASA contract NAS 5-26555.

REFERENCES

- Allgood, B., Flores, R. A., Primack, J. R., Kravtsov, A. V., Wechsler, R. H., Faltenbacher, A., & Bullock, J. S. 2005, MNRAS, submitted (astro-ph/0508497)
- Bender, R., & Möllenhoff, C. 1987, A&A, 177, 71
- Bender, R., Surma, P., Döbereiner, S., Möllenhoff, C., & Madejsky, R. 1989, A&A, 217, 35
- Berlind, A. A., & Weinberg, D. H. 2002, ApJ, 575, 587
- Bernardi, M., et al. 2003, AJ, 125, 1849
- Bullock, J. S., Kravtsov, A. V., & Weinberg, D. H. 2000, ApJ, 539, 517
- Chiba, M. 2002, ApJ, 565, 17
- Chiba, M., Minezaki, T., Kashikawa, N., Katata, H., & Inoue, K. T. 2005, ApJ, 627, 53
- Congdon, A. B., & Keeton, C. R. 2005, MNRAS, in press (astro-ph/0510232)
- Cooray, A., & Sheth, R. 2002, Phys. Rept., 372, 1
- Courbin, F., Magain, P., Keeton, C. R., Kochanek, C. S., Vanderriest, C., Jaunsen, A. O., & Hjorth, J. 1997, A&A, 324, 1
- Dalal, N., & Kochanek, C. S. 2002, ApJ, 572, 25
- Eigenbrod, A., Courbin, F., Dye, S., Meylan, G., Sluse, D., Saha, P., Vuissoz, C., & Magain, P. 2005, A&A, submitted (astro-ph/0510641)
- Evans, N. W., & Witt, H. J. 2001, MNRAS, 327, 1260
- Evans, N. W., & Witt, H. J. 2003, MNRAS, 345, 1351
- Falco, E. E., et al. 1999, ApJ, 523, 617
- Gao, L., White, S. D. M., Jenkins, A., Stoehr, F., & Springel, V. 2004, MNRAS, 355, 819
- Impey, C. D., Falco, E. E., Kochanek, C. S., Lehár, J., McLeod, B. A., Rix, H.-W., Peng, C. Y., & Keeton, C. R. 1998, ApJ, 509, 551
- Inada, N., et al. 2003, AJ, 126, 666
- Katz, N. 1991, ApJ, 368, 325
- Keeton, C. R., & Kochanek, C. S. 1997, ApJ, 487, 42
- Keeton, C. R., Kochanek, C. S., & Seljak, U. 1997, ApJ, 482, 604
- Keeton, C. R., & Zabludoff, A. I. 2004, ApJ, 612, 660
- Keeton, C. R., Burles, S., Schechter, P. L., & Wambsganss, J. 2005, ApJL, submitted (astro-ph/0507521)
- King, L. J., Browne, I. W. A., Muxlow, T. W. B., Narasimha, D., Patnaik, A. R., Porcas, R. W., & Wilinon, P. N. 1997, MNRAS, 289, 450
- King, L. J., et al. 1998, MNRAS, 295, L41
- Kravtsov, A. V., Gnedin, O. Y., & Klypin, A. A. 2004, ApJ, 609, 482
- Klypin, A., Kravtsov, A. V., Valenzuela, O., & Prada, F. 1999, ApJ, 522, 82
- Kochanek, C. S. 2003, ApJ, 583, 49
- Kochanek, C. S., & Dalal, N. 2004, ApJ, 610, 69
- Kochanek, C. S., Keeton, C. R., & McLeod, B. A. 2001, ApJ, 547, 50
- Kochanek, C. S., Morgan, N. D., Falco, E. E., McLeod, B. A., Winn, J. N., Dembicky, J., & Ketzeback, B. 2005, ApJ, submitted (astro-ph/0508070)
- Koopmans, L. V. E., & Treu, T. 2003, ApJ, 583, 606
- Kravtsov, A. V., Berlind, A. A., Wechsler, R. H., Klypin, A. A., Gottlöber, S., Allgood, B., & Primack, J. R. 2004, ApJ, 509, 35
- Lehár, J., et al. 2000, ApJ, 536, 584
- Mao, S., & Schneider, P. 1998, MNRAS, 295, 587
- McLeod, B. A. 1997, in 1997 HST Calibration Workshop, ed. S. Casertano et al., Space Telescope Institute, 281
- Metcalf, R. B., & Zhao, H.-S. 2002, ApJ, 567, L5
- Morgan, N. D., Kochanek, C. S., Pevunova, O., & Schechter, P. L., 2005, AJ, 129, 2531
- Moore, B., Ghigna, S., Governato, F., Lake, G., Quinn, T., Stadel, J., & Tozzi, P. 1999, ApJ, 524, L19
- Ofek, E. O., Maoz, D., Rix, H.-W., Kochanek, C. S., & Falco, E. E. 2005, ApJ, submitted (astro-ph/0510465)
- Oguri, M., et al. 2004, ApJ, 605, 78
- Press, W. H., Flannery, B. P., Teukolsky, S. A., & Vetterling, W. T. 1992, Numerical Recipes (Cambridge: Cambridge Univ. Press)
- Rest, A., van den Bosch, F. C., Jaffe, W., Tran, H., Tsvetanov, Z., Ford, H. C., Davies, J., & Schafer, J. L. 2001, AJ, 121, 2431
- Ros, E., Guirado, J. C., Marcaide, J. M., Pérez-Torres, M. A., Falco, E. E., Muñoz, J. A., Alberdi, A., & Lara, L. 2000, A&A, 362, 845
- Rusin, D., & Kochanek, C. S. 2005, ApJ, 623, 666
- Rusin, D., et al. 2003a, ApJ, 587, 143
- Rusin, D., Kochanek, C. S., & Keeton, C. R. 2003b, ApJ, 595, 29
- Schechter, P. L., et al. 1997, ApJ, 475, L85
- Seljak, U. 2000, MNRAS, 318, 203
- Taylor, J. E., & Babul, A. 2004, MNRAS, submitted (astro-ph/0410048)
- Tonry, J. L., & Kochanek, C. S. 2000, AJ, 119, 1078
- Treu, T., & Koopmans, L. V. E. 2002, ApJ, 575, 87
- Trotter, C. S., Winn, J. N., & Hewitt, J. N. 2000, ApJ, 535, 671
- van den Bosch, F. C., Weinmann, S. M., Yang, X., Mo, H. J., Li, C., & Jing, Y. P. 2005, MNRAS, submitted (astro-ph/0502466)
- Weymann, R. J., et al. 1980, Nature, 285, 641
- Wisotzki, L., Christlieb, N., Bade, N., Beckmann, V., Köhler, T., Vanelle, C., & Reimers, D. 2000, A&A, 358, 77
- Wucknitz, O. 2002, MNRAS, 332, 951
- Yoo, J., Kochanek, C. S., Falco, E. E., & McLeod, B. A. 2005, ApJ, 626, 51
- Zentner, A. R., Berlind, A. A., Bullock, J. S., Kravtsov, A. V., & Wechsler, R. H. 2005, ApJ, 624, 505
- Zheng, Z., et al. 2005, ApJ, in press (astro-ph/0408564)

Zhao, H. S., & Pronk, D. 2001, MNRAS, 320, 401